Fidelity of adaptive phototaxis

Knut Drescher, Raymond E. Goldstein[1], and Idan Tuval

Department of Applied Mathematics and Theoretical Physics, University of Cambridge, Wilberforce Road, Cambridge CB3 0WA, United Kingdom

Edited by Harry L. Swinney, University of Texas, Austin, TX, and approved May 6, 2010 (received for review January 28, 2010)

Along the evolutionary path from single cells to multicellular organisms with a central nervous system are species of intermediate complexity that move in ways suggesting high-level coordination, yet have none. Instead, organisms of this type possess many autonomous cells endowed with programs that have evolved to achieve concerted responses to environmental stimuli. Here experiment and theory are used to develop a quantitative understanding of how cells of such organisms coordinate to achieve phototaxis, by using the colonial alga *Volvox carteri* as a model. It is shown that the surface somatic cells act as individuals but are orchestrated by their relative position in the spherical extracellular matrix and their common photoresponse function to achieve colony-level coordination. Analysis of models that range from the minimal to the biologically faithful shows that, because the flagellar beating displays an adaptive down-regulation in response to light, the colony needs to spin around its swimming direction and that the response kinetics and natural spinning frequency of the colony appear to be mutually tuned to give the maximum photoresponse. These models further predict that the phototactic ability decreases dramatically when the colony does not spin at its natural frequency, a result confirmed by phototaxis assays in which colony rotation was slowed by increasing the fluid viscosity.

adaptation | evolution | flagella | fluid dynamics | multicellularity

The most primitive "eyes" evolved long before brains and even before the simplest forms of nervous system organization appeared on Earth (1, 2). Many organisms are able to sense and respond to light stimuli, an ability essential to the optimization of photosynthesis, the avoidance of photodamage, and the use of light as a regulatory signal. One of the more striking responses is phototaxis, in which motile photosynthetic microorganisms adjust their swimming path with respect to incident light in a finely tuned manner (3, 4). This steering relies on sensory inputs from one or more eyespots (2), primitive photosensors that are among the simplest and most common "eyes" in nature. They consist of photoreceptor proteins and an optical system of varying complexity, which provide information about the intensity and directionality of the incident light (2, 3, 5). This information is then translated into an organism-specific swimming control mechanism that allows orientation to the light with high fidelity.

In most unicellular phototactic organisms, such as the archetypal green alga *Chlamydomonas*, the presence of a single eyespot implies both a limited vision of the three-dimensional world in which the cell navigates and the impossibility of detecting light directions by measuring light intensity at two different positions in the cell body. To overcome these restrictions, such organisms must compare light intensity measurements from their single eyespot at different moments in time (6). Many species do this by swimming on helical paths along which their eyespot acts as a light antenna continuously searching space for bright spots (3). Higher eukaryotes have a nervous system to integrate visual information from different sources and orchestrate coordinated responses (7, 8).

Multicellular organisms of intermediate complexity, such as the colonial alga *Volvox* and its relatives (9), have evolved a means of high-fidelity phototaxis without a central nervous system and, in many cases, even in the absence of intercellular communication through cytoplasmic connections (10). *Volvox carteri* consists of thousands of biflagellated *Chlamydomonas*-like somatic cells sparsely distributed at the surface of a passive spherical extracellular matrix, and a small number of germ cells inside the sphere (Fig. 1*A*). During development the flagella orient such that *Volvox* rotates about its swimming direction, the trait that gave *Volvox* its name (11). Coordination of the somatic cells resembles orchestrating a rowboat with thousands of independent rowers but without a coxswain (9). Nature's solution is a response program at the single-cell level that produces an accurate steering mechanism, an emergent property at the colonial level. Yet it remains to be understood what form the response program must take to coordinate the cells and to yield high-fidelity phototaxis in the presence of the steering constraints of a viscous environment.

More than a century ago, Holmes (12) proposed that the somatic cells facing a source of light down-regulate their flagellar activity, a hypothesis later confirmed by several investigators (13–16). Although this control principle will initially turn the colony towards the light, the colony might adapt (14, 15) to the light before good alignment with the light direction has been reached. Surprisingly, this observation has not been synthesized into a predictive, quantitative model consistent with the principles of fluid dynamics, nor are there data on *Volvox* phototaxis that can be compared with such a theory. Here we use a combination of experiment and theory to show that adaptation and colony rotation play key roles in the phototaxis mechanism of *V. carteri*. By quantifying the flagellar photoresponse of *V. carteri* in detail, we show that it acts as a band pass filter that allows adaptation to different light environments, minimizes the influence of fast light fluctuations, and maximizes the response to stimuli at frequencies that correspond to the rotation rate of the organism. These measurements suggest that the response kinetics and colony rotation have evolved to be mutually tuned and optimized for phototaxis. Furthermore, we develop a mathematical theory that predicts the phototactic fidelity of *Volvox* as the rotation rate and other parameters change and confirm experimentally that colony rotation is essential for accurate phototaxis.

Results and Discussion

Temporal Dynamics of the Adaptive Response. The most elementary photoresponse is the change in flagellar beating accompanying a step up or down in illumination intensity. This response is probed with the experimental setup shown in Fig. 1*B*. Cyan light from an LED that is coupled to a fiber-optic light guide held in a micropipette is directed toward the anterior of a *V. carteri* colony held by a second micropipette. Details are given in *Materials and Methods* and *SI Text*. High-speed imaging of flagella revealed, in accord with proposals by several investigators (13–15), that the somatic cells change their beating frequency rather than their beating direction (17). Instead of quantifying the average photoresponse by recording the beating frequency of each flagellum of

Author contributions: K.D., R.E.G., and I.T. designed research; K.D., R.E.G., and I.T. performed research; K.D. analyzed data; and K.D., R.E.G., and I.T. wrote the paper.

The authors declare no conflict of interest.

This article is a PNAS Direct Submission.

[1]To whom correspondence should be addressed. E-mail: R.E.Goldstein@damtp.cam.ac.uk.

This article contains supporting information online at www.pnas.org/lookup/suppl/doi:10.1073/pnas.1000901107/-/DCSupplemental.

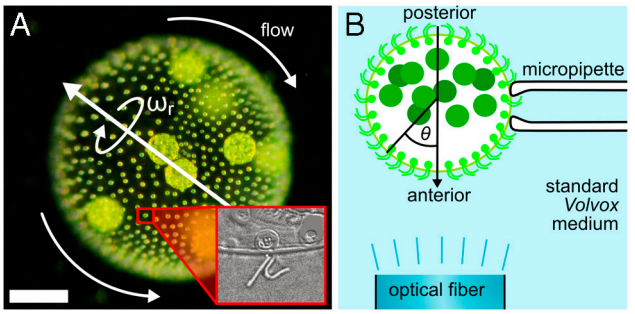

Fig. 1. Geometry of *V. carteri* and experimental setup. (*A*) The beating flagella, two per somatic cell (*Inset*), create a fluid flow from the anterior to the posterior, with a slight azimuthal component that rotates *Volvox* about its posterior-anterior axis at angular frequency ω_r. (Scale bar: 100 μm.) (*B*) Studies of the flagellar photoresponse utilize light sent down an optical fiber.

every somatic cell, we measured the fluid motion produced by the flagellar beating by using particle image velocimetry (PIV). This approach implicitly averages over several neighboring flagella, and, by measuring the fluid velocity just above the flagellar tips, we obtain a natural input for the hydrodynamic models of phototactic turning described further below. Because of the low Reynolds number associated with flows generated by *V. carteri* (18–20), fluid inertia is negligible and the flagella-induced flow is a direct measure of the flagellar activity. Fig. 2*A* shows a typical time trace of the photoresponse, measured in terms of the flagella-generated flow speed $u(t)$, normalized by the flow speed under time-independent illumination u_0, and averaged over ±30° from the anterior pole. We found that a step up in light intensity elicits a decrease in flagellar activity on a response time scale τ_r, followed by a recovery to baseline activity on a time scale τ_a

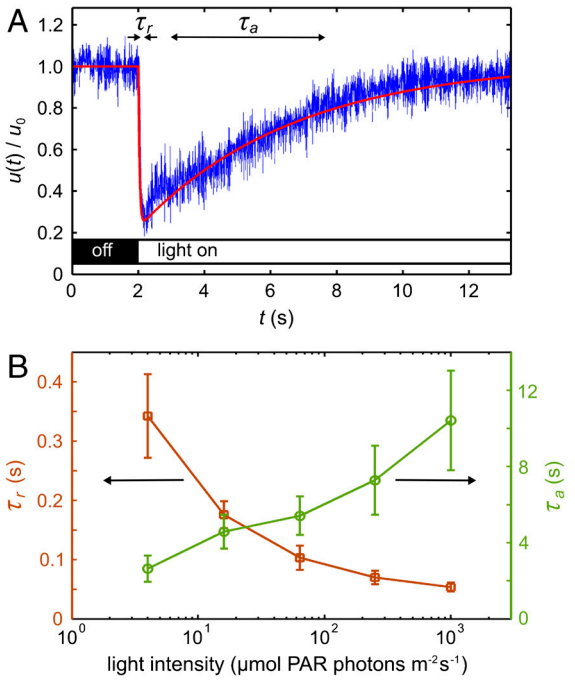

Fig. 2. Characteristics of the adaptive photoresponse. (*A*) The local flagella-generated fluid speed $u(t)$ (*Blue*), measured with PIV just above the flagella during a step up in light intensity, serves as a measure of flagellar activity. The baseline flow speed in the dark is $u_0 = 81$ μm/s for this dataset. Two time scales are evident: a short response time τ_r and a longer adaptation time τ_a. The fitted theoretical curve (*Red*) is from Eq. **4**. (*B*) The times τ_r (*Squares*) and τ_a (*Circles*) vary smoothly with the stimulus light intensity, measured in terms of PAR. Error bars are standard deviations.

associated with adaptation; there was no change in flagellar activity upon a step down in light intensity. This response underlies the ability of *V. carteri* to turn toward the light, as explained further below. At very high light intensities and long stimulation, the responses to step up and step down stimuli are reversed (see *SI Text*), allowing *Volvox* to avoid photodamage by swimming away from the light. Irrespective of the stimulus light intensity, τ_r is always a fraction of a second, whereas τ_a is several seconds (Fig. 2*B*), consistent with early observations (14, 15).

Although the kinetics and biochemistry of photoreceptor currents have been studied in *Chlamydomonas* (2, 21) and *Volvox* (22), their connection to the flagellar photoresponse is unclear. In *Volvox*, a step stimulus elicits a Ca^{2+} current whose time scale of 1 ms (22) is too short to account for the measured τ_r. But the time for Ca^{2+} to diffuse the length of the flagellum L is $\tau_D = L^2/D \sim 0.2$ s (for $L \sim 15$ μm, $D \sim 10^{-5}$ cm^2/s), which is similar to τ_r, suggesting that the photocurrent triggers an influx of Ca^{2+} at the base of the flagella, consistent with previous hypotheses (22, 23). Although the dependence of τ_a on light intensity is like that of the H^+ current in *Volvox*, the decay constant of the latter is only ~75 ms (22); the biochemical origin of τ_a remains unknown.

The measured adaptive response of the flagella-generated fluid speed just above the colony surface (Fig. 2*A*) can be described by $u(t)/u_0 = 1 - \beta p(t)$, where $p(t)$ is a dimensionless photoresponse variable that is large when there is a large light-induced decrease in flagellar activity and vanishes when there is no such change in flagellar activity. The empirically determined constant $\beta > 0$ quantifies the amplitude of the decrease in $u(t)/u_0$. For a model of $p(t)$ that captures the two time scales τ_a and τ_r, we require a second variable $h(t)$, which we define as a dimensionless representation of the hidden internal biochemistry responsible for adaptation (24, 25). A system of coupled equations that is consistent with the measured $u(t)/u_0$ is

$$\tau_r \dot{p} = (s-h)H(s-h) - p, \quad [1]$$

$$\tau_a \dot{h} = s - h, \quad [2]$$

where the light stimulus $s(t)$ is a dimensionless measure of the photoreceptor input that incorporates the eyespot directionality. The Heaviside step function $H(s-h)$ is used to ensure that a step down in light stimulus cannot increase u above u_0, because it keeps $p \geq 0$. In these equations, the values $p^* = 0$ and $h^* = s_1$ are stable and global attractors in the sense that, after a sufficiently long time under constant light stimulus s_1, the pair (p, h) relaxes to (p^*, h^*). However, if s increases from s_1 for $t < 0$ to s_2 for $t \geq 0$, then for $t > 0$ the solution is

$$h(t) = s_1 e^{-t/\tau_a} + s_2(1 - e^{-t/\tau_a}), \quad [3]$$

$$p(t) = \frac{(s_2 - s_1)}{1 - \tau_r/\tau_a}(e^{-t/\tau_a} - e^{-t/\tau_r}). \quad [4]$$

When $\tau_r \ll \tau_a$, as for *Volvox*, there is a sharp transient increase in $p(t)$ [and decrease in $u(t)$], peaking at a time $t^\dagger \sim \tau_r \ln(\tau_a/\tau_r)$, followed by a slow relaxation back to zero, as in the measured flagellar photoresponse shown in Fig. 2*A*.

The rotation of *Volvox* about its axis and the resulting periodic illumination of the photoreceptors suggest an investigation of the dependence of the photoresponse on the frequency of sinusoidal stimulation. For the above model this frequency dependence of the photoresponse is $\mathcal{R} = |\tilde{p}/\tilde{s}|$, where $\tilde{p}$ and $\tilde{s}$ are the Fourier transforms of p and s, respectively. $\mathcal{R}$ is well-approximated by neglecting the Heaviside function in Eq. **1** (see *SI Text*) to give

$$\mathcal{R}(\omega_s) = \frac{\omega_s \tau_a}{\sqrt{(1+\omega_s^2\tau_r^2)(1+\omega_s^2\tau_a^2)}}. \quad [5]$$

If the stimulus angular frequency ω_s is very low ($\omega_s \ll 2\pi/\tau_a$), the adaptive process has sufficient time to keep up with the changing light levels and the amplitude of the response vanishes. At very high frequencies, $\omega_s \gg 2\pi/\tau_r$, the response is limited to short-time behavior and also vanishes.

Using the setup in Fig. 1*B*, we measured the flagellar photoresponse to sinusoidal light stimuli of various temporal frequencies. In Fig. 3*A*, these measurements are compared with the theoretical $\mathcal{R}(\omega_s)$, showing excellent agreement. The maximum response is obtained at stimulus frequencies that correspond to the natural angular rotation frequencies of *Volvox* about its swimming direction. The frequency dependence of the photoresponse is like a band pass filter that removes high frequency noise, e.g., light fluctuations from ripples on the water surface (26), but retains the key feature of adaptation.

Heuristic Mechanism of Phototaxis. We proceed to a qualitative discussion of how an adaptive response translates into phototactic turning and the ingredients required for a simple yet realistic mathematical model with predictive power.

In general, phototactic orientation is due to an asymmetry of the flagellar behavior between the illuminated and shaded sides of the organism. The mechanism that achieves this asymmetry is species-dependent, but it is instructive to consider a hierarchy of ingredients. First, consider a nonspinning spherical organism that can display a nonadaptive photoresponse on its entire surface but will do so only on the illuminated side, as in Fig. 4*A*. This organism will achieve perfect antialignment of its posterior-anterior axis $\mathbf{k}$ with the light direction unit vector $\hat{\mathbf{I}}$ (i.e., face the light) on a turning time scale τ_t, which is determined by the balance between the torques due to asymmetric flagellar activity and rotational viscous drag. Adaptation to light is a desirable property for such an organism, because it allows a response to light intensities over several orders of magnitude and because it allows the organism to swim at full speed once a good orientation has been reached. If the photoresponse of the above model organism now has the desirable property of being adaptive, it will initially turn towards the light as in Fig. 4*A*, but adaptation may cause the response to decay before $\mathbf{k}$ reaches antialignment with $\hat{\mathbf{I}}$ (Fig. 4*B*), depending on the relative magnitude of τ_a and τ_t. If, however, the adaptive organism would spin about $\mathbf{k}$, new surface area would continuously be exposed, thus maintaining an asymmetric photoresponse until perfect antialignment of $\mathbf{k}$ with $\hat{\mathbf{I}}$ has been reached. For *Volvox*, which generally have $\tau_a \sim \tau_t$, the spinning about the posterior-anterior axis is therefore not just optimized for the photoresponse kinetics, as shown in the previous section, but also essential for high-fidelity phototactic orientation in the presence of adaptation. Spinning may also mitigate the deleterious effects of unsymmetrical colony development and injury (27), and for organisms with a restricted field of view due to a small number of eyespots, such as *Chlamydomonas* and *Platynereis*, spinning is also required for detecting the light direction (3, 7).

In *Volvox* colonies, the flagellar photoresponse is localized near the anterior pole (Fig. 5), yet the importance of spinning outlined above remains. However, having only a small photoresponsive region complicates the heuristic picture: If the eyespots could only direct an all-or-nothing response as they move from the shaded to the illuminated side of the sphere, the best possible phototactic orientation is drawn in Fig. 4*C*. Such a mechanism

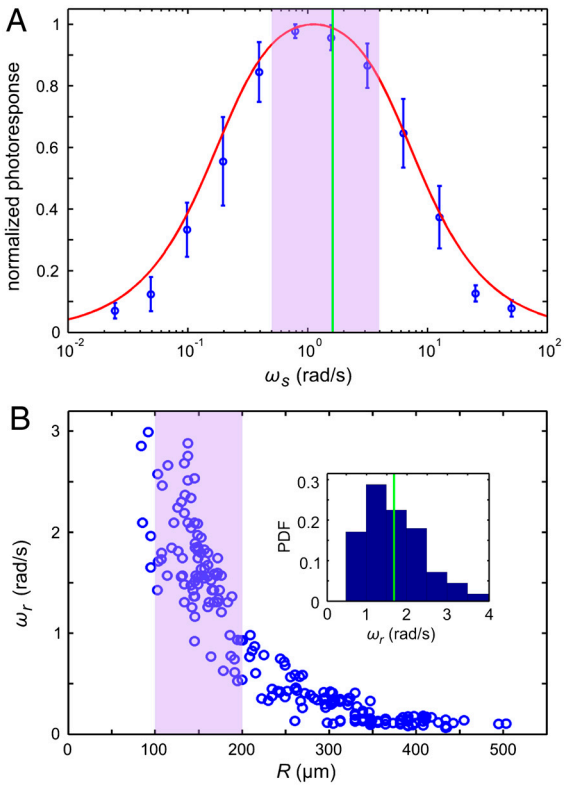

Fig. 3. Photoresponse frequency dependence and colony rotation. (*A*) The normalized flagellar photoresponse for different frequencies of sinusoidal stimulation, with minimal and maximal light intensities of 1 and 20 μmol PAR photons m^{-2} s^{-1} (*Blue Circles*). The theoretical response function (Eq. **5**, *Red Line*) shows quantitative agreement, using τ_r and τ_a from Fig. 2*B* for 16 μmol PAR photons m^{-2} s^{-1}. (*B*) The rotation frequency ω_r of *V. carteri* as a function of colony radius *R*. The highly phototactic organisms for which photoresponses were measured fall within the range of *R* indicated by the purple box, and the distribution of *R* can be transformed into an approximate probability distribution function (PDF) of ω_r (*Inset*), by using the noisy curve of $\omega_r(R)$. The purple box in *A* marks the range of ω_r in this PDF (green line indicates the mean), showing that the response time scales and colony rotation frequency are mutually optimized to maximize the photoresponse.

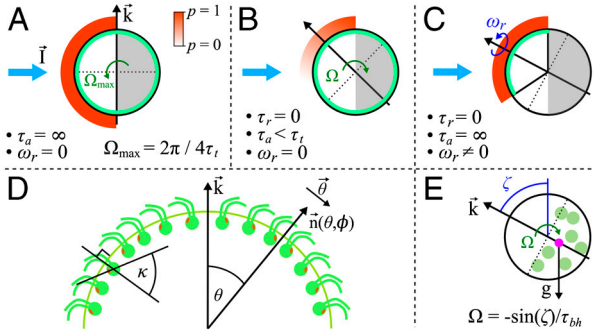

Fig. 4. Heuristic analysis of the phototactic fidelity. *A–C* illustrate simplified phototaxis models. Photoresponsive regions are colored green, the region that actually displays a photoresponse is in shades of red, and shaded regions are gray. (*A*) If $\tau_a = \infty$, $\omega_r = 0$, and the responsive region is as drawn, the posterior-anterior axis $\mathbf{k}$ will achieve perfect antialignment with the light direction $\mathbf{I}$. The time scale for turning $\tau_t \sim 3.3$ s can be estimated by assuming that the fluid velocity on the illuminated side is reduced to 0.7 of its baseline value and using Eq. **8** without bottom-heaviness. (*B*) If $\tau_a < \tau_t$, and $\omega_r = 0$, the photoresponse may decay before the optimal orientation has been reached. After the initial transient in *A* has decayed, the largest photoresponse (i.e., flagellar down-regulation) is in the region that just turned into the light. As an illustration, the configuration drawn in this panel surprisingly implies that the organism would turn away from the light, indicating that before this orientation is reached the steering is stopped at a suboptimal orientation of $\mathbf{k}$ with $\mathbf{I}$. A remedy against this orientational limitation would be $\omega_r \neq 0$. (*C*) The best attainable orientation towards the light is drawn, if the photoresponse is localized in a small anterior region, and the eyespots display an all-or-nothing response as they move from the shaded to the illuminated side. (*D*) Measurements of the eyespot (*Orange*) placement yield $\kappa = 57° \pm 7°$ (see *SI Text*). (*E*) *Volvox* is bottom-heavy, because the center of mass (*Pink*) is offset from the geometric center of the colony as indicated.

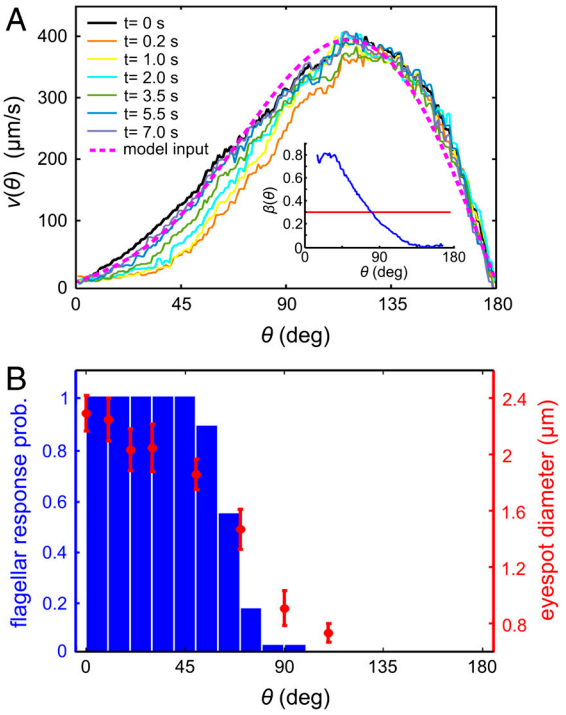

Fig. 5. Anterior-posterior asymmetry. (*A*) The anterior-posterior component of the fluid flow, measured 10 μm above the beating flagella, following a step up in illumination at time $t = 0$ s. The dashed line indicates the approximation to $v_0(\theta)$ used in the numerical model. (*Inset*) $\beta(\theta)$ is blue (with p normalized to unity), and the mean β is red. (*B*) The probability of flagella to respond to light correlates with the size of the somatic cell eyespots. The light-induced decrease in fluid flow occurs beyond the region of flagellar response because of the nonlocality of fluid dynamics.

may be sufficient for *Volvox* in natural environments, because it would robustly navigate *Volvox* closer to the light, even though the organism does not swim directly toward the light. The orientational limit of this response mechanism can be overcome if, as described for several green algae (3, 28, 29), the strength of the photoresponse instead continuously changes with the angle at which the eyespots receive light. Together with an appropriate eyespot placement (Fig. 4*D*), this directionality leads to the persistence of a response asymmetry between illuminated and shaded regions until perfect orientation toward the light has been achieved.

Phototactic orientation in natural environments can be opposed by ambient vorticity (30), which may be created by the motion of other nearby organisms, convection, or wind-driven surface waves. A mechanism that can counteract phototaxis even in well-controlled laboratory experiments is due to a property that *Volvox* shares with its unicellular ancestor *Chlamydomonas* and other algae: Their center of mass is offset from their center of buoyancy. For *Volvox*, this bottom-heaviness is due to clustering of germ cells in the posterior (Fig. 4*E*) and leads to a torque tending to align the swimming direction with the vertical on a time scale $\tau_{bh} \sim 14$ s (20). A faithful theory of phototaxis in *Volvox* must therefore include at least four features: self-propulsion, bottom-heaviness, photoresponse kinetics, and photoresponse spatial structure.

Hydrodynamic Model of Phototaxis. In the low Reynolds number regime that *Volvox* inhabits, the swimming speed and angular velocity $\mathbf{\Omega}$ of an organism can be calculated if the fluid velocity $\mathbf{u}$ on each point of its surface is known (31). Phototactic steering of *Volvox* can therefore be modeled by specifying the response of $\mathbf{u}$ to light stimulation. Rather than solving for the effects of each of the thousands of individual flagella on the colony surface, we adopt a continuum approximation in which there is a temporally and spatially varying surface velocity. If θ and ϕ are the polar and azimuthal angles on a sphere, respectively, the surface velocity $\mathbf{u}$ may be decomposed into $\mathbf{u} = v\hat{\boldsymbol{\theta}} + w\hat{\boldsymbol{\phi}}$. We interpret $\mathbf{u}$ as the velocity at the edge of the flagellar layer (32); for practical reasons experimental measurements of $\mathbf{u}$ are made just above that layer. In the absence of a light stimulus, $\mathbf{u} = \mathbf{u}_0$ and we assume that the ratio $v_0(\theta)/w_0(\theta)$ is constant on the colony surface because of the precise orientational order of somatic cells (9). Following step changes in light intensity, measurements of $v(\theta,\phi,t)$ at fixed ϕ show that in each region, the surface velocity displays a photoresponse of the form shown in Fig. 2*A* but that the overall magnitude varies with θ (Fig. 5*A*). We thus model $\mathbf{u}(\theta,\phi,t)$ by allowing the quantities β, p, and h to depend on position:

$$\mathbf{u}(\theta,\phi,t) = \mathbf{u}_0(\theta)[1 - \beta(\theta)p(\theta,\phi,t)]. \quad [6]$$

The measured $\beta(\theta)$ is shown in the inset in Fig. 5*A*.

To define the stimulus s on the colony surface, we make use of the angle $\psi(\theta,\phi,\hat{\mathbf{I}})$ defined through $\cos\psi = -\hat{\mathbf{n}}\cdot\hat{\mathbf{I}}$, where $\hat{\mathbf{n}}$ is the unit normal to the surface. When $\psi = 0$ (π), the light is directly above (behind) a given surface patch. The light-shadow asymmetry in s can therefore be modeled by a factor $H(\cos\psi)$. Superimposed on this factor may be another functional dependence on ψ to account for the eyespot sensitivity in the forward direction, with experiments on *Chlamydomonas* (28) supporting a dependence $f(\psi) = \cos\psi$. The class of models we consider for the dimensionless s is therefore

$$s(\theta,\phi,\hat{\mathbf{I}}) = f(\psi)H(\cos\psi). \quad [7]$$

With the above specification of the dynamics of the surface velocity, the angular velocity of the colony is (31)

$$\mathbf{\Omega}(t) = \frac{1}{\tau_{bh}}\hat{\mathbf{g}}\times\hat{\mathbf{k}} - \frac{3}{8\pi R^3}\int \hat{\mathbf{n}}\times\mathbf{u}(\theta,\phi,t)dS, \quad [8]$$

where $\hat{\mathbf{g}}$ and $\hat{\mathbf{k}}$ are the directions of gravity and the posterior-anterior axis, respectively. The first term in Eq. **8** arises from bottom-heaviness and represents a balance between the torque that acts when the posterior-anterior axis is not parallel to gravity and the rotational drag of the sphere (20). The second term is responsible for phototactic steering, where the integral is taken over the surface of the sphere of radius R. In a reference frame where the *Volvox* is at the origin with a fixed orientation, the light direction evolves as $d\hat{\mathbf{I}}/dt = -\mathbf{\Omega}\times\hat{\mathbf{I}}$.

The above coupled equations can be solved numerically (see *SI Text*), e.g., to determine the angle $\alpha(t)$ of the organism axis with the light direction. It is interesting to consider two special cases of the model class outlined above. In the biologically faithful "full model," we use the measured $\beta(\theta)$ and the realistic eyespot directionality $f(\psi) = \cos\psi$. In the "reduced model," we consider only a light-shadow response asymmetry—i.e., $f(\psi) = 1$—and use the mean of the measured $\beta(\theta)$—i.e., $\beta(\theta) = 0.3$. All other features are shared between the models.

A phototactic turn of a hypothetical non-bottom-heavy *Volvox* simulated by the reduced model is shown in Fig. 6, indicating an intricate link between organism rotation, adaptation, and steering. In reality, however, *Volvox* is bottom-heavy, which is particularly important when the light direction is horizontal. In this case, we previously observed (33) that the organisms reach a final angle α_f set by the balance of the bottom-heaviness torque and the phototactic torque. We therefore define the "phototactic ability" $\mathcal{A}$ = (swimming speed toward the light)/(swimming speed).

Both models predict that as the viscosity η is increased, while keeping the internal parameters τ_r and τ_a fixed, the phototactic ability decreases dramatically (Fig. 7). Qualitatively, an increase in η reduces ω_r, which leads to a reduced photoresponse (Fig. 3*A*)

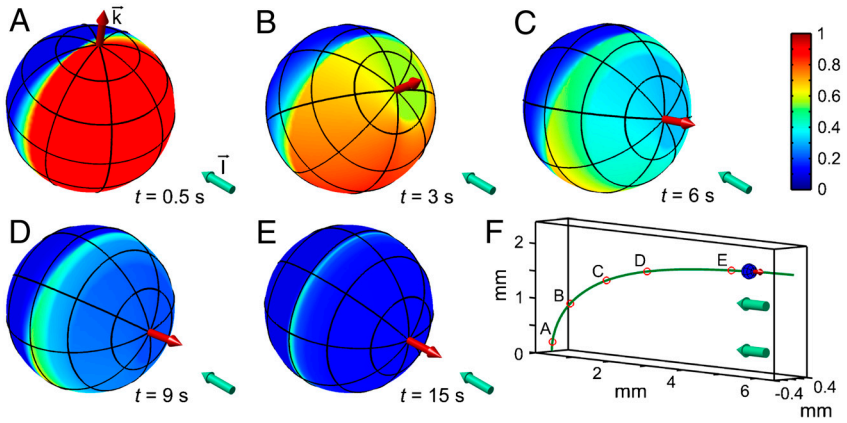

Fig. 6. Colony behavior during a phototurn. *A–E* show the colony axis **k** (*Red Arrow*) tipping toward the light direction **l** (*Aqua Arrow*). Colors represent the amplitude $p(t)$ of the down-regulation of flagellar beating in a simplified model of phototactic steering. *F* shows the location of colonies in *A–E* along the swimming trajectory.

and therefore a reduced phototactic torque. The sharp transition in Fig. 7 occurs when the phototactic torque becomes comparable to the other torques in the system. The simulations neglected torques due to ambient fluid motion and included only the bottom-heaviness torque.

We tested the above prediction by measuring the phototactic ability of *Volvox* at various viscosities in a population assay at low organism concentration and negligible ambient fluid motion. It is important to note that, in the experiment, the phototactic ability is a measure of a slightly different quantity than in the model. In the model, a bottom-heavy *Volvox* swims in an infinite fluid toward the light at an angle α_f with the horizontal. A colony swimming in the same direction in the experiment will collide with the top surface of the sample and change direction. The phototactic ability in the experiments is therefore a measure of the directionality of the population swimming behavior (see *SI Text*), whereas in the model it is solely a measure of α_f. The data from several populations are shown in Fig. 7 and are found to be in quantitative agreement with the full model for realistic parameters (given in *SI Text*) and in qualitative agreement with the reduced model. The success of the reduced model highlights that spinning and adaptation are the key ingredients for a qualitative understanding

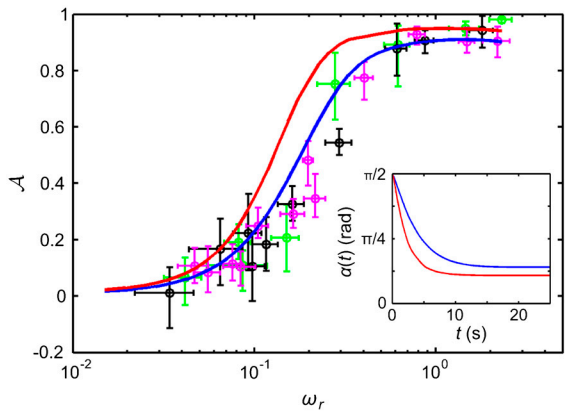

Fig. 7. The phototactic ability $\mathcal{A}$ decreases dramatically as ω_r is reduced by increasing the viscosity. Results from three representative populations are shown with distinct colors. Each data point represents the average phototactic ability of the population at a given viscosity. Horizontal error bars are standard deviations, whereas vertical error bars indicate the range of population mean values, when it is computed from 100 random selections of 0.1% of the data. A blue continuous line indicates the prediction of the full hydrodynamic model; the red line is obtained from the reduced model. (*Inset*) $\alpha(t)$ from the full and reduced model at the lowest viscosity.

of the fidelity of phototaxis in *Volvox* and that a quantitative understanding can be obtained if a realistic eyespot directionality and anterior-posterior response asymmetry are included. These models further illustrate that if all somatic cells were photoresponsive, the organism would have a higher phototactic ability (Fig. 7). Yet it may be beneficial to keep a high translation speed even during light stimulation, and there may be significant metabolic and developmental costs associated with endowing all cells with a photoresponse, which could make it advantageous to have the photoresponse localized in the anterior.

In additional experiments, we found that very large *Volvox* (Fig. 3*B*) have a much lower phototactic ability although they still display the flagellar photoresponse. For such colonies, the hydrodynamic model (Eq. **8**) reveals that their lower phototactic ability arises from the increase in R and concomitant decrease in u_0, and the reduction in photoresponse p due to the lower ω_r (Fig. 3*A*). The model thus yields insight into which parameters determine the phototactic torque and illustrates the intuitive result that this torque must be significantly larger than competing torques to achieve high-fidelity phototaxis.

Conclusion

We have shown how accurate phototaxis of the alga *V. carteri*, a colonial organism lacking a central nervous system, is achieved by autonomous cells on its anterior surface endowed with an adaptive flagellar photoresponse. The response and adaptation time scales of this photoresponse determine an optimal frequency for the characteristic spinning of *Volvox* about its swimming direction. Because the organisms naturally spin at this optimal frequency, the flagellar orientation and photoresponse kinetics seem to have coevolved to maximize the photoresponse. The mathematical model of phototaxis developed here shows that the phototactic fidelity decreases dramatically when the colony does not spin at its natural frequency; the results of a phototaxis assay in which spinning was slowed by increasing the fluid viscosity are in excellent agreement with the model predictions.

This work raises a number of issues for further investigation. Chief among them are the biochemical origin of the adaptive time scale and the reason for displaying a photoresponse only in the anterior part of the organism. Because the rotational frequency of phototactically active *V. carteri* so closely matches the peak of the frequency response function $\mathcal{R}(\omega)$, and *Chlamydomonas* itself displays a coincidence of its photoresponse and rotation period (34, 35), it is natural to ask whether other species in the same evolutionary lineage, or indeed the larger class of phototactic organisms, can be understood within the present formalism. The allometry of the adaptation time is therefore a key feature for study. It is also of considerable interest to ascertain the

dynamics of chemotaxis in *Volvox* and to determine its relationship to phototaxis, a linkage proposed for *Chlamydomonas* (36). Whereas larger multicellular organisms like *Volvox* can rely on an entirely deterministic mechanism for phototaxis, it remains unclear how stochasticity of motion in unicellular organisms like *Chlamydomonas*, caused by internal biochemical noise (37), affects phototaxis. Finally, the interplay between adaptive flagellar dynamics and the vorticity of natural fluid environments (30) requires further investigation.

Materials and Methods

A detailed description of materials, methods, and supplementary measurements is given in *SI Text*. A brief summary is given below.

Culture Conditions. *V. carteri* f. *nagariensis* EVE strain was grown axenically in standard *Volvox* medium (SVM) with sterile air bubbling, in a daily cycle of 16 h of cool white light (4,000 lx) at 28 °C and 8 h of darkness at 26 °C.

Measuring the Photoresponse to Various Stimuli. *Volvox* colonies were caught on a rotatable micropipette by gentle aspiration and rotated until the posterior-anterior axis was in the focal plane of the microscope and pointing toward an optical fiber at a distance of ∼900 μm. Microscopy was done in red bright-field illumination ($\lambda > 620$ nm), to which *Volvox* is insensitive (15). The flagella-generated flow was visualized with 1-μm polystyrene beads ($\sim 1.4 \times 10^8$ beads per mL in SVM) and recorded at 100 fps. Flow speeds were measured by PIV. The PIV data was interpolated and read out 25 μm above the colony surface—i.e., approximately 10 μm above the flagellar layer. To get a single time series that represents the photoresponse of the colony, we averaged the flow speed time series between −30° and +30° as measured from the anterior pole. All stimuli were applied with a cyan LED (500 nm, FWHM 40 nm) coupled into a 550 μm diameter optical fiber. LabVIEW was used to trigger the camera and control the LED light intensity time series. The temperature in the sample chamber was 24.5 ± 0.5 °C.

Measuring the Rotation Rate Dependence of the Phototactic Ability. We prepared solutions of SVM with various concentrations of methylcellulose (M0512, Sigma-Aldrich UK), up to 0.65% (wt/wt) (38). From a *V. carteri* culture that just hatched, phototactic organisms were preselected by a simple test and distributed into rectangular Petri dishes with different concentrations of methylcellulose in SVM. A cyan LED (same as for the optical fiber stimuli) was placed on one side of each Petri dish, providing ∼15 μmol photosynthetically active radiation (PAR) photons $m^{-2}\,s^{-1}$. The *Volvox* were tracked with software written in Matlab, and rotation frequencies were measured manually. The temperature in the Petri dishes was 24 ± 1 °C.

ACKNOWLEDGMENTS. We thank J.P. Gollub, J.T. Locsei, C.A. Solari, S. Ganguly, and T.J. Pedley for discussions and D. Page-Croft and J. Milton for technical assistance. This work was supported in part by the Engineering and Physical Sciences Research Council (K.D.), the Engineering and Biological Sciences program of the Biotechnology and Biological Sciences Research Council, the Human Frontier Science Program (I.T.), the US Department of Energy, and the Schlumberger Chair Fund (R.E.G.).

1. Gehring WJ (2005) New perspectives on eye development and the evolution of eyes and photoreceptors. *J Hered* 96:171–184.
2. Hegemann P (2008) Algal sensory photoreceptors. *Annu Rev Plant Biol* 59:167–189.
3. Foster KW, Smyth RD (1980) Light antennas in phototactic algae. *Microbiol Rev* 4:572–630.
4. Jékely G (2009) Evolution of phototaxis. *Philos Trans R Soc B* 364:2795–2808.
5. Kreimer G (1994) Cell biology of phototaxis in algae. *Int Rev Cytol* 148:229–310.
6. Sineshchekov OA, Govorunova EG (2001) Rhodopsin receptors of phototaxis in green flagellate algae. *Biochemistry-Moscow* 66:1300–1310.
7. Jékely G, et al. (2008) Mechanism of phototaxis in marine zooplankton. *Nature* 456:395–399.
8. Egelhaaf M, Kern R (2002) Vision in flying insects. *Curr Opin Neurobiol* 12:699–706.
9. Kirk DL *Volvox: Molecular-Genetic Origins of Multicellularity and Cellular Differentiation* (Cambridge Univ Press, Cambridge, UK).
10. Hiatt JDF, Hand WG (1972) Do protoplasmic connections function in phototactic coordination of the *Volvox* colony during light stimulation? *J Protozool* 19:488–489.
11. Linnaeus C (1758) *Systema Naturae* (Laurentii Salvii, Stockholm), 10th Ed p 820.
12. Holmes SJ (1903) Phototaxis in *Volvox. Biol Bull* 4:319–326.
13. Hand WG, Haupt W (1971) Flagellar activity of the colony members of *Volvox aureus* Ehrbg during light stimulation. *J Protozool* 18:361–364.
14. Huth K (1970) Movement and orientation of *Volvox aureus* Ehrbg (translated from German). *Z Pflanzenphysiol* 62:436–450.
15. Sakaguchi H, Iwasa K (1979) Two photophobic responses in *Volvox carteri. Plant Cell Physiol* 20:909–916.
16. Hoops HJ, Brighton MC, Stickles SM, Clement PR (1999) A test of two possible mechanisms for phototactic steering in *Volvox carteri* (Chlorophyceae). *J Phycol* 35:539–547.
17. Mast SO (1926) Reactions to light in *Volvox*, with special reference to the process of orientation. *Z Vergl Physiol* 4:637–658.
18. Solari CA, Ganguly S, Kessler JO, Michod RE, Goldstein RE (2006) Multicellularity and the functional interdependence of motility and molecular transport. *Proc Natl Acad Sci USA* 103:1353–1358.
19. Short MB, et al. (2006) Flows driven by flagella of multicellular organisms enhance long-range molecular transport. *Proc Natl Acad Sci USA* 103:8315–8319.
20. Drescher K, et al. (2009) Dancing *Volvox*: Hydrodynamic bound states of swimming algae. *Phys Rev Lett* 102:168101.
21. Harz H, Hegemann P (1991) Rhodopsin-regulated calcium currents in *Chlamydomonas. Nature* 351:489–491.
22. Braun F-J, Hegemann P (1999) Two light-activated conductances in the eye of the green alga *Volvox carteri. Biophys J* 76:1668–1678.
23. Tamm S (1994) Ca^{2+} channels and signalling in cilia and flagella. *Trends Cell Biol* 4:305–310.
24. Friedrich BM, Jülicher F (2007) Chemotaxis of sperm cells. *Proc Natl Acad Sci USA* 104:13256–13261.
25. Spiro PA, Parkinson JS, Othmer HG (1997) A model of excitation and adaptation in bacterial chemotaxis. *Proc Natl Acad Sci USA* 94:7263–7268.
26. Walsh P, Legendre L (1983) Photosynthesis of natural phytoplankton under high frequency light fluctuations simulating those induced by sea surface waves. *Limnol Oceanogr* 28:688–697.
27. Jennings HS (1901) On the significance of the spiral swimming of organisms. *Am Nat* 35:369–378.
28. Schaller K, David R, Uhl R (1997) How *Chlamydomonas* keeps track of the light once it has reached the right phototactic orientation. *Biophys J* 73:1562–1572.
29. Schaller K, Uhl R (1997) A microspectrophotometric study of the shielding properties of eyespot and cell body in *Chlamydomonas. Biophys J* 73:1573–1578.
30. Durham WM, Kessler JO, Stocker R (2009) Disruption of vertical motility by shear triggers formation of thin phytoplankton layers. *Science* 323:1067–1070.
31. Stone HA, Samuel ADT (1996) Propulsion of microorganisms by surface distortions. *Phys Rev Lett* 77:4102–4104.
32. Blake JR (1971) A spherical envelope approach to ciliary propulsion. *J Fluid Mech* 46:199–208.
33. Drescher K, Leptos KC, Goldstein RE (2009) How to track potists in three dimensions. *Rev Sci Instrum* 80:014301.
34. Yoshimura K, Kamiya R (2001) The sensitivity of *Chlamydomonas* photoreceptor is optimized for the frequency of cell body rotation. *Plant Cell Physiol* 42:665–672.
35. Josef K, Saranak J, Foster KW (2006) Linear systems analysis of the ciliary steering behavior associated with negative-phototaxis in *Chlamydomonas reinhardtii. Cell Motil Cytoskeleton* 63:758–777.
36. Ermilova EV, Zalutskaya ZM, Gromov BV, Häder D-P, Purton S (2000) Isolation and characterization of chemotactic mutants of *Chlamydomonas reinhardtii* obtained by insertional mutagenesis. *Protist* 151:127–137.
37. Polin M, Tuval I, Drescher K, Gollub JP, Goldstein RE (2009) *Chlamydomonas* swims with two 'gears' in a eukaryotic version of run-and-tumble locomotion. *Science* 325:487–490.
38. Herraez-Dominguez JV, Gil Garcia de Leon F, Diez-Sales O, Herraez-Dominguez M (2005) Rheological characterization of two viscosity grades of methylcellulose: An approach to the modeling of the thixotropic behaviour. *Colloid Polym Sci* 284:86–91.

Supporting Information

Drescher et al. 10.1073/pnas.1000901107

SI Text

Culture Conditions. For all experiments, we used *Volvox carteri* f. *nagariensis* EVE strain, a subclone of the HK10 strain, kindly provided by A.M. Nedelcu (University of New Brunswick) and D.L. Kirk (Washington University, St. Louis). *V. carteri* were grown axenically in 50 ml of standard *Volvox* medium (SVM) (1, 2) in 125-mL Erlenmeyer flasks with sterile air bubbling. Experiments were performed with cultures that were grown up to a concentration of ~200 colonies per mL, after inoculating the culture with ~50 colonies. For the population assay, more organisms were required so that *V. carteri* were grown in 125 mL of SVM in 250-mL Erlenmeyer flasks. The culture flasks were kept in diurnal growth chambers (KBW400; Binder GmbH), where they were illuminated from above by cool white fluorescent light, in a daily cycle of 16 h of light at 28 °C and 8 h of darkness at 26 °C. The intensity of the growth light was ~4,000 lx, or 80 μmol of photosynthetically active radiation (PAR; light with wavelengths between 400 and 700 nm) photons $m^{-2}\,s^{-1}$ (see spectrum in Fig. S1).

Stimuli with an Optical Fiber. A schematic diagram of the sample chamber is given in Fig. S2*A*. The bottom and top surfaces are made from glass coverslips. The vertical spacer is a 3.2-mm outer diameter plastic tube glued to the glass by UV-curing optical glue (NOA68; Norland Products). The geometry of the chamber allows easy access from two perpendicular directions, as in Fig. S2*B*. The temperature was monitored by a thermistor attached to the sample chamber and found to be 24.5 ± 0.5 °C. All measurements were done in SVM.

To keep a *Volvox* colony in the field of view of the microscope for extended periods, it was caught with a micropipette by aspiration. The micropipettes were pulled from glass capillaries, shaped, and fire polished (with equipment from Sutter Instrument) to have a rounded tip of outer diameter ~100 μm, as in Fig. S2*B*. The untreated end of the micropipette was then inserted into a holder (PicoNozzle; World Precision Instruments), connected to a gas-tight syringe with micrometer control (Manual Injector; Sutter). The micropipette/holder assembly was mounted on a custom-made rotation stage, attached to a motorized micromanipulator (PatchStar; Scientifica). To stimulate reliably only the anterior part of a *Volvox* colony, it was necessary to rotate the micropipette until the anterior-posterior axis of the colony was in the focal plane. After some practice it was possible to catch organisms with their posterior-anterior axis approximately perpendicular to the axis of the micropipette, allowing a reorientation of the colony by pipette rotation to an orientation as shown in Fig. S2*B*. The anterior-posterior axis was found to be in the focal plane when the germ cells were grouped on one side of the colony (so that in the focal plane, the area of a polygon that encloses the projections of the germ cells is minimal) and when at the same time the posterior pole (as identified by the position of the germ cells) is opposite to the anterior flow stagnation point (as identified by inspection of the self-generated flow). The flow was visualized with 1-μm carboxylate-modified polystyrene beads (F8819; Invitrogen), suspended in SVM at a concentration of $\sim 1.4 \times 10^8$ beads per mL. Movies of the flow in response to a stimulus time series were recorded at 100 fps with a high-speed camera (Phantom V5.1; Vision Research), connected directly to a Nikon TE2000-U inverted microscope with a Nikon 10× (N.A. 0.3) objective in bright-field illumination. To avoid photoresponses due to the halogen lamp bright-field illumination (3–7), two identical long pass interference filters (each with a 10-nm transition between transmissions of $T = 10^{-3}$ and $T = 0.8$, centered at 620 nm; Knight Optical) were placed in the microscope beam path.

All stimuli were applied with a cyan LED (Luxeon V; Philips Lumileds; see spectrum in Fig. S1), coupled into a 550-μm-diameter optical fiber (N.A. 0.22, FG550LEC; Thorlabs) via a fiber launch station (MBT611/M; Thorlabs) with a 10× (N.A. 0.25) Olympus objective. The fiber was fed through a micropipette holder (PicoNozzle; World Precision Instruments) that was attached to a micromanipulator identical to the one used to control the micropipette position. The amount of light leaving the free end of the fiber was measured with a photodiode (DET110; Thorlabs) and could be controlled manually with an iris in the fiber-coupling beam path and electronically by sending modulation voltages (0–5 V) to the LED driver (LEDD1; Thorlabs). The electronic control allowed time-dependent stimuli to be produced with a time resolution better than 1 ms. The modulation voltage time series that provided the stimulus time series were written in LabVIEW and contained a triggering signal for the high-speed camera.

Flow speeds were measured from the recorded movies by particle image velocimetry (PIV), with an open source software package for Matlab (8). The PIV data were interpolated so that flow speeds could be read out 25 μm above the colony surface—i.e., approximately 10 μm above the flagellar layer. To get a single time series that represents the photoresponse of the colony, we averaged the flow speed time series between the angles −30° and +30° as measured from the anterior pole.

Measuring the frequency response. We supplied a sinusoidal light stimulus to the organism anterior, with a minimum light intensity of 1 μmol PAR photons $m^{-2}\,s^{-1}$ and a maximum of 20 μmol PAR photons $m^{-2}\,s^{-1}$. These values were chosen to be consistent with the population assay described below. Because the output of the LED was not quite linear in the modulation voltage, we calibrated the modulation voltage time series in such a way that the light intensity time series was sinusoidal. As the very onset of light emission was difficult to calibrate reliably, we chose to have a nonzero minimum light intensity. For each stimulus, the organism was stimulated for 30 s (or two periods, whichever was longer) directly before the recording began. Yoshimura and Kamiya (9) assumed that, to simulate the organism rotation for a *Chlamydomonas* cell, the most realistic stimulus would be a "half-sine"—i.e., a stimulus proportional to $H(\sin \omega_s t) \sin \omega_s t$, where H, ω_s, and t are the Heaviside step function, stimulus angular frequency, and time, respectively. In addition to using a sinusoidal stimulus, as shown in Fig. 3 of the main text, we also measured the photoresponse to half-sine stimuli. The data for both stimuli are compared in Fig. S3. It is evident that at low ω_s the high Fourier frequency content of the half-sine leads to a higher response, in comparison to the purely sinusoidal stimulus, where only a single frequency is present. For each organism, the responses were normalized by the organism's maximum response. The normalized responses were averaged across 16 organisms for the sinusoidal stimulus and 25 organisms for the half-sine stimulus.

Measuring the photoresponse for different light intensities. We measured the photoresponse as a function of the stimulus light intensity, for a stimulus frequency of 0.25 Hz. Instead of a sinusoidal stimulus we used a top-hat function, because this allowed the minimum light intensity to be zero. The organism was dark-adapted between each stimulus (i.e., movie) for 2 min. At each light intensity, the organism was stimulated with 20 periods before the recording began, and the response was recorded for

4 periods. When the flagellar beating (i.e., the measured flow speed) decreased upon an increasing stimulus light, the photoresponse was termed "positive" because it turns the organism toward the light, as discussed in the main text. A photoresponse was termed "negative" when the flagella beating decreased upon a decrease in stimulus light, because this will turn the organism away from the light. Negative photoresponses could be modeled with a similar dynamical system as the positive photoresponses, including the Heaviside function, so that we expect our theory to also hold for negative phototaxis. The transition from positive to negative phototaxis occurred between 100–250 μmol PAR photons m^{-2} s^{-1}. Interestingly, when organisms were dark-adapted, they displayed positive photoresponses even for the highest light intensities in the first ∼30 s of the stimulus time series and then switched to negative phototaxis. The response amplitude was taken as the amplitude of the oscillatory signal. For each organism, the responses were normalized by the organism's maximum response. The normalized responses were averaged across 16 organisms. A graph of the photoresponse as a function of stimulus intensity is shown in Fig. S4.

Measuring the two time scales. For this measurement *V. carteri* colonies were dark-adapted for at least 2 min and then exposed to a sharp increase in stimulus light intensity. The response was characterized with two time scales: the response and adaptation time scales. The model response was fitted to the flow speed time series to obtain τ_r and τ_a. The time scales were measured for 20 organisms.

Measuring the flagellar response probability. For this measurement we observed the flagellar behavior directly rather than observing the flow generated by the flagella. This allowed a more precise localization of the light-responsive region on the *V. carteri* colony. To visualize flagella, the high-speed camera recorded images at 200 fps, in red bright-field illumination ($\lambda > 620$ nm, obtained with filters as described above) using a Nikon 40× (N.A. 0.6) air objective. The organism was held on a rotatable micropipette, in the same geometry as in Fig. S2*B*, except that now the posterior pole was nearest to the optical fiber. The stimuli were a large step up in light intensity (from 0 to 1500 μmol PAR photons m^{-2} s^{-1}) and a corresponding step down 6 s later. Such a strong stimulus assured that even the somatic cells on the far side of the colony, as viewed from the optical fiber (i.e., those near the anterior pole), received a strong enough stimulus to display a significant photoresponse. A whole *Volvox* colony has been measured to attenuate light of 490 nm by a factor of ∼2 (10), and an individual *Chlamydomonas* cell (which is similar to a *Volvox* somatic cell) has been measured to attenuate light of 495 nm by a factor of ∼8 (11, 12), yielding a minimum stimulus amplitude on the far side of the colony of ∼90 μmol PAR photons m^{-2} s^{-1}. A "response" was defined as a change in the flagellar beating period (periods were measured manually) following a step stimulus. Often the flagella slowed down so much that they stopped completely, as previously described by Gerisch (13) and Huth (10). Because the axis of the organism was in the focal plane, we could measure at which polar angles θ (where $\theta = 0$ is the anterior pole) a *V. carteri* colony is responsive to light. This measurement was performed on 35 young colonies, just after they hatched.

Measuring the Eyespot Size. A *V. carteri* colony was caught and held with a micropipette, using the same equipment and sample chamber as described above. To obtain high resolution images of the somatic cells and their eyespots, a Nikon 60× (N.A. 1.4) oil objective with differential interference contrast optics was used. Photographs were taken with a digital single-lens reflex camera (Nikon D300) directly connected to the microscope. The *V. carteri* colonies were caught with their posterior-anterior axis almost exactly perpendicular to the axis of the micropipette. By rotating the holding micropipette and focusing on the colony surface, it was thus possible to move the anterior pole into the focal plane (see Fig. S5*A*). By rotating further, while keeping the focus on the colony surface, the eyespot size could be measured as a function of the polar angle θ (see Fig. S5*B*). In the images of the eyespots, the largest diameter was taken to be the eyespot size. For $\theta \gtrsim 110°$, eyespots could not be clearly distinguished within the somatic cells, and eyespot sizes are thus not given for these angles. Measurements were performed on 10 young colonies, just after they hatched. The somatic cells are precisely arranged in each colony (14–16). For all colonies, the images showed that the center of a somatic cell and the center of the eyespot are at the same longitude (Fig. S5 *A* and *B*), and that within a somatic cell the eyespot is placed further away from the anterior pole than the center of the somatic cell.

To gain further information on the eyespot placement in the somatic cells, we observed the somatic cells on the *Volvox* perimeter while the posterior-anterior axis was in the focal plane (the organism orientation was as in Fig. S2*B*). This yielded photographs similar to the schematic diagram in Fig. S5*C*. These photographs allowed us to measure the angle κ (defined in Fig. S5*C*). For these measurements we ignored a possible dependence of κ on θ.

Measuring the Rotation Rate Dependence of the Phototactic Ability. For measurement of the phototactic ability as a function of the rotation frequency of *V. carteri*, we devised a population assay as follows. To control the rotation frequency we prepared solutions of SVM with various concentrations of methylcellulose (M0512; Sigma-Aldrich), the highest concentration being 0.65% (weight/weight). The macroscopic rheology of methylcellulose has been determined to be Newtonian at concentrations <1% (17). Rectangular Petri dishes (11.7 × 7.5 cm, Nunc 242811; Thermo Fisher Scientific) were then filled with 30 mL of SVM containing different concentrations of methylcellulose (yielding a bath of depth ∼3.5 mm).

At the beginning of a series of measurements to assess the phototactic ability at the various viscosities, a whole *V. carteri* culture that just hatched was removed from its Erlenmeyer flask in the growth chamber and placed into a custom-made large rectangular dish with a light on one side (the same type of LED we used for the stimuli delivered with an optical fiber). This light was used to select phototactic organisms (almost all colonies displayed strong phototaxis at this stage), which were placed into the rectangular Petri dish of a particular viscosity (and mixed on an orbital shaker for 4 min) just before the measurement. In this way, the phototactic ability was measured for organisms from the same culture, at different viscosities (and thus rotation rates). Pipetting was done slowly to avoid high shear rates which could rip flagella off the *V. carteri* surface.

To measure the phototactic ability, individual *V. carteri* colonies were tracked while the stimulus light was on. The schematic diagram in Fig. S6*A* illustrates the geometry of the experimental setup. A CCD camera (Pike F145B; Allied Vision Technologies) attached to a long working distance microscope (InfiniVar CFM-2/S; Infinity Photo-Optical) recorded movies at various frame rates (triggering was done through a pulse train generated with LabVIEW). The bright-field background illumination for the microscope was provided by a red LED (maximum at 655 nm, FWHM 21 nm, LFR-100-R; CCS Inc.). The light intensity that the stimulus light source provided in the field of view of the camera was measured to be ∼15 μmol PAR photons m^{-2} s^{-1}, yielding positive phototaxis. During the assay, temperature was measured with a thermistor attached to the rectangular Petri dishes and found to be in the range 24 ± 1 °C.

To obtain the phototactic ability, we computed the cosine of the angle of the swimming track with the light direction of each organism at every time step. The distribution of swimming angles with the light direction is given for two very different viscosities in

Fig. S6 *B* and *C*. Rotation rates were measured manually with the aid of a commercial image processing software (MetaMorph; Molecular Devices) by counting frames. For each viscosity and population, we measured ω_r for 20 colonies.

Details of the Mathematical Model. The mathematical model for phototaxis of *Volvox* relies only on measured parameters and is able to give detailed predictions of the swimming characteristics and the ability to turn toward the light. It is based on a knowledge of the fluid velocity at the edge of the flagellar layer of *Volvox* and how this fluid velocity changes when parts of the surface are exposed to a light stimulus.

The coupled equations that make up the model are given in the main text. To determine the time evolution of the system of coupled equations, we solved the coupled partial differential equations for $p(\theta,\phi,t)$ and $h(\theta,\phi,t)$ numerically with a built-in solver in Mathematica (Wolfram Research) between times t and $t+\delta t$. Due to the integral in the equation for $\mathbf{\Omega}$, we used an Euler method to then solve the equation for $\hat{\mathbf{I}}(t)$ at every time step. We ensured convergence of the results by choosing a small enough step size δt.

In addition to finding the angle of the *Volvox* axis with the light direction, the model can also be used to determine the organism swimming velocity $\mathbf{U}$, via another result from Stone and Samuel (18)

$$\mathbf{U}(t) = \frac{1}{4\pi R^2}\int \mathbf{u}(\theta,\phi,t)dS, \qquad \textbf{[S1]}$$

which allows trajectories of the organism to be reconstructed.

A solution of the photoresponse $p(\theta,\phi,t)$ is plotted in Fig. 6 of the main text, using the "reduced model" defined in the main text. A decomposition of this photoresponse into spherical harmonics $Y_l^m(\theta,\phi)$ is given in Fig. S7. The photoresponse p computed by the "full model" during a phototactic turn is shown in Fig. S8, neglecting bottom-heaviness.

The initial conditions of the model were a horizontal light direction, an upward-pointing posterior-anterior axis, and $p = h = 0$. The input parameters for the model are the following measurable quantities:

- R, the *Volvox* radius. For the simulations we used $R = 140$ μm, the mean of the populations we investigated experimentally.
- U, the translational swimming speed, which fixes the amplitude of v_0. For the simulations we used $U = 390$ μm/s, the mean of the populations we investigated experimentally.
- ω_r, the rotation rate without a light stimulus, which fixes the amplitude of w_0. For the simulations we used $\omega_r = 2.3$ rad/s, as shown in Fig. 7 of the main text.
- The θ dependence of the surface velocity. For the simulations we approximated $v_0(\theta)$ by a superposition of two associated Legendre functions, $-P_1^1(\cos\theta) + 0.25P_2^1(\cos\theta)$, as shown by the dashed magenta line in Fig. 5 of the main text. Using a simple $\sin\theta$ dependence for $v_0(\theta)$ gives qualitatively similar results. We assume that w_0 has the same θ dependence as v_0.
- $\beta(\theta)$, the responsivity of the fluid flow to light stimulation. For the full model, we used a close approximation to the $\beta(\theta)$ shown in the inset in Fig. 5*A* of the main text. For the reduced model, we used $\beta(\theta) = 0.3$, the mean of the $\beta(\theta)$ used for the full model.
- τ_r and τ_a, the response and adaptation time scales, respectively. For the simulations, we used the values measured for a light intensity of 16 μmol PAR photons $\mathrm{m}^{-2}\,\mathrm{s}^{-1}$, as displayed in Fig. 2*B* of the main text.
- τ_{bh}, the bottom-heaviness time scale, is defined by considering a flagellaless *Volvox* that is tilted at an angle ζ from the vertical. The axis of this *Volvox* would relax back to the vertical at a rate $\dot{\zeta} = -\sin(\zeta)/\tau_{\mathrm{bh}}$. For the simulations, we used $\tau_{\mathrm{bh}} = 14$ s, as measured in ref. 19.

In order to compare the results from this mathematical model with the measurements of the phototactic ability as a function of viscosity, we implemented a viscosity dependence in the model. For this we defined $\mathbf{u} = [\mathbf{u}]_w\eta_w/\eta$ and $\tau_{\mathrm{bh}} = [\tau_{\mathrm{bh}}]_w\eta/\eta_w$, where η is the viscosity and the subscript w denotes values in water.

1. Kirk DL, Kirk MM (1983) Protein synthetic patterns during the asexual life cycle of *Volvox carteri*. *Dev Biol* 96:493–506.
2. Solari CA, Ganguly S, Kessler JO, Michod RE, Goldstein RE (2006) Multicellularity and the functional interdependence of motility and molecular transport. *Proc Natl Acad Sci USA* 103:1353–1358.
3. Sakaguchi H, Iwasa K (1979) Two photophobic responses in *Volvox carteri*. *Plant Cell Physiol* 20:909–916.
4. Schletz K (1976) Phototaxis in Volvox—Pigments involved in the perception of light direction. *Z Pflanzenphysiol* 77:189–211.
5. Halldal P (1958) Action spectra of phototaxis and related problems in Volvocales, *Ulva* gametes and Dinophyceae. *Physiol Plant* 11:118–153.
6. Mast SO (1917) The relation between spectral color and stimulation in the lower organism. *J Exp Zool* 22:471–528.
7. Sineshchekov OA, Jung K-H, Spudich JL (2002) Two rhodopsins mediate phototaxis to low- and high-intensity light in *Chlamydomonas reinhardtii*. *Proc Natl Acad Sci USA* 99:8689–8694.
8. MatPIV is an open source PIV software toolbox written for Matlab. Downloads and details are at http://www.math.uio.no/~jks/matpiv/.
9. Yoshimura K, Kamiya R (2001) The sensitivity of *Chlamydomonas* photoreceptor is optimized for the frequency of cell body rotation. *Plant Cell Physiol* 42:665–672.
10. Huth K (1970) Movement and orientation of *Volvox aureus* Ehrbg. (translated from German). *Z Pflanzenphysiol* 62:436–450.
11. Harz H, Hegemann P (1991) Rhodopsin-regulated calcium currents in *Chlamydomonas*. *Nature* 351:489–491.
12. Schaller K, Uhl R (1997) A microspectrophotometric study of the shielding properties of eyespot and cell body in *Chlamydomonas*. *Biophys J* 73:1573–1578.
13. Gerisch G (1959) Cellular differentiation in *Pleodorina californica* and the organisation of colonial Volvocales (translated from German). *Arch Protistenkunde* 104:292–358.
14. Hoops HJ (1993) Flagellar cellular and organismal polarity in *Volvox carteri*. *J Cell Sci* 104:105–117.
15. Coggin SJ, Kochert G (1986) Flagellar development and regeneration in *Volvox carteri* (Chlorophyta). *J Phycol* 22:370–381.
16. Huskey RJ (1979) Mutants affecting vegetative cell orientation in *Volvox carteri*. *Dev Biol* 72:236–243.
17. Herraez-Dominguez JV, Gil Garcia de Leon F, Diez-Sales O, Herraez-Dominguez M (2005) Rheological characterization of two viscosity grades of methylcellulose: An approach to the modeling of the thixotropic behaviour. *Colloid Polym Sci* 284:86–91.
18. Stone HA, Samuel ADT (1996) Propulsion of microorganisms by surface distortions. *Phys Rev Lett* 77:4102–4104.
19. Drescher K, et al. (2009) Dancing *Volvox*: Hydrodynamic bound states of swimming algae. *Phys Rev Lett* 102:168101.
20. Solari CA, Kessler JO, Michod RE (2006) A hydrodynamics approach to the evolution of multicellularity: Flagellar motility and germ-soma differentiation in Volvocalean green algae. *Am Nat* 167:537–554.

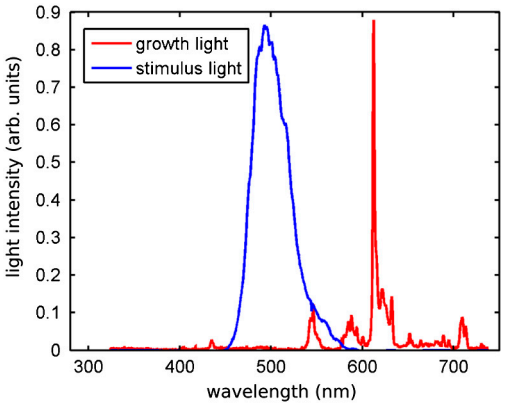

Fig. S1. Spectra of growth and stimulus light sources.

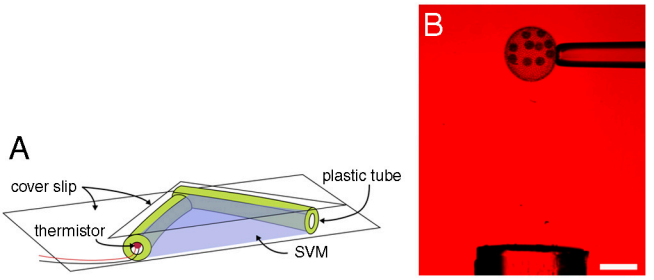

Fig. S2. (*A*) Schematic diagram of the sample chamber. (*B*) Photograph of a micropipette holding a *V. carteri* colony and the optical fiber. The colony axis is in the focal plane and pointing toward the fiber. (Scale bar: 200 μm.)

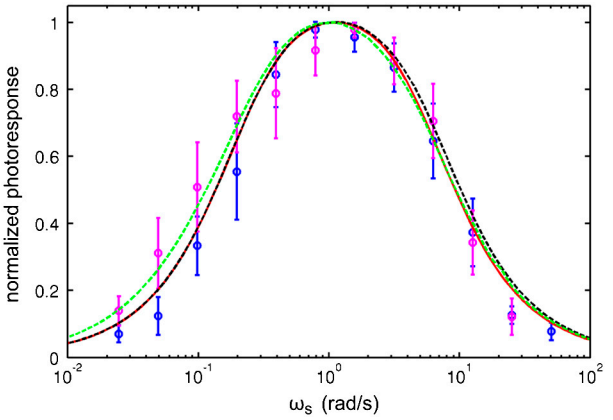

Fig. S3. Photoresponse of *V. carteri* as a function of stimulus frequency. Measurements with a sinusoidal stimulus are displayed as blue circles, measurements with a half-sine stimulus are displayed as magenta circles. The red line is a plot of Eq. **5** in the main text and therefore neglects the Heaviside function in the simple model (Eqs. **1** and **2** in the main text). The black dashed line indicates a numerical evaluation of the simple model for a sinusoidal stimulus, including the Heaviside function. The green dashed line indicates a numerical evaluation of the simple model for a half-sine stimulus, also including the Heaviside function.

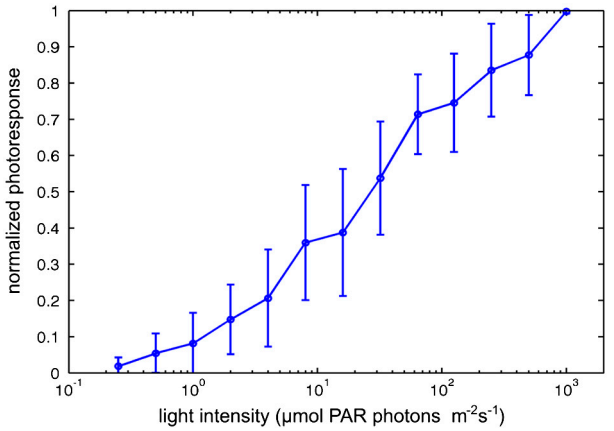

Fig. S4. The amplitude of the photoresponse for top-hat stimuli of frequency 0.25 Hz, at different stimulus light intensities.

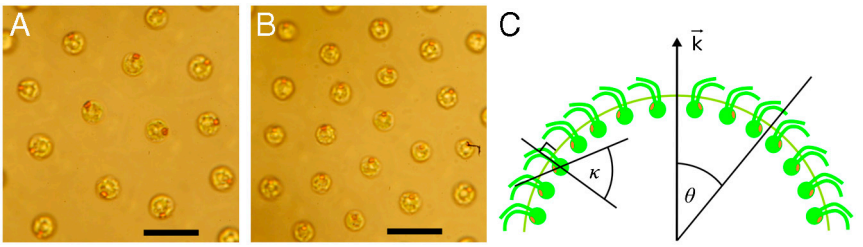

Fig. S5. (*A*) The *V. carteri* somatic cells at the anterior pole have their orange eyespots facing away from the fluid-mechanical anterior pole. (*B*) The somatic cells and eyespots at polar angle $\theta = 50°$ from the anterior. (Scale bars: 20 μm.) (*C*) Illustration of the eyespot placement in the somatic cells and the relation to the posterior-anterior axis **k**. In contrast to this schematic drawing, *V. carteri* colonies consist of thousands of somatic cells, as shown in Fig. 1*A* of the main text and as measured in ref. 20.

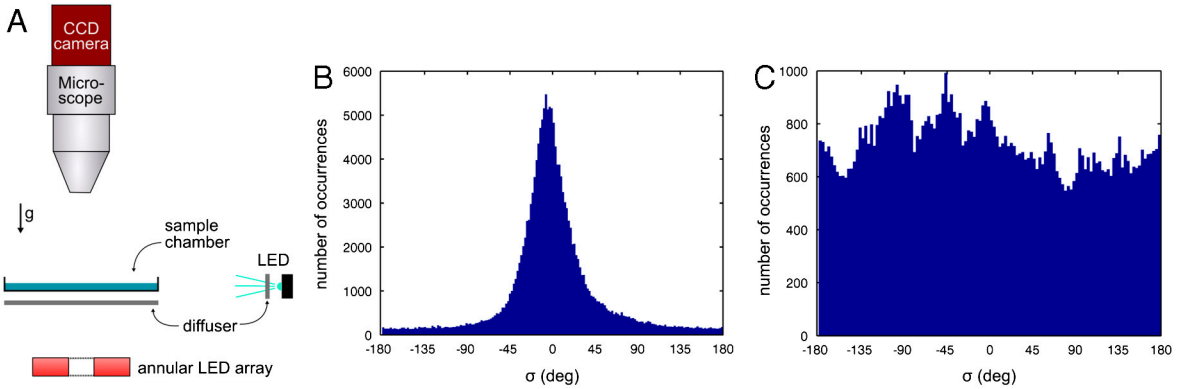

Fig. S6. (*A*) Schematic diagram of the apparatus used for the population assay. *B* and *C* show distributions of the swimming angle with the light direction σ as measured for a population at the viscosity of water (*B*) and at 40 times the viscosity of water (*C*).

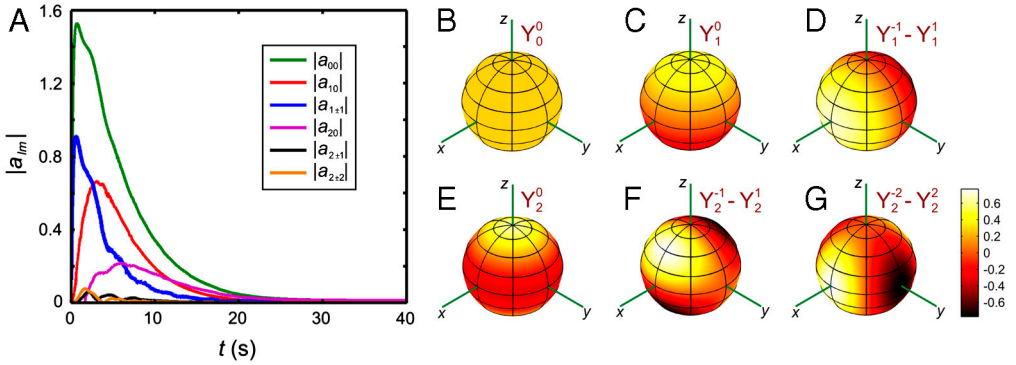

Fig. S7. The photoresponse p may be decomposed into the spherical harmonics $Y_l^m(\theta,\phi)$ via the equation $p(\theta,\phi,t) = \sum_{l,m} a_{lm}(t) Y_l^m(\theta,\phi)$. The decomposition was done for the photoresponse shown in Fig. 6 of the main text–i.e., using the reduced model. For this model, the dominant modes are the constant Y_0^0, the $Y_1^{\pm 1}$ modes that give a ϕ dependence similar to the light-shadow asymmetry, and Y_1^0, which gives an anterior-posterior asymmetry that becomes important in this model when the organism has turned significantly toward the light. *B–G* display the spherical harmonics on a sphere.

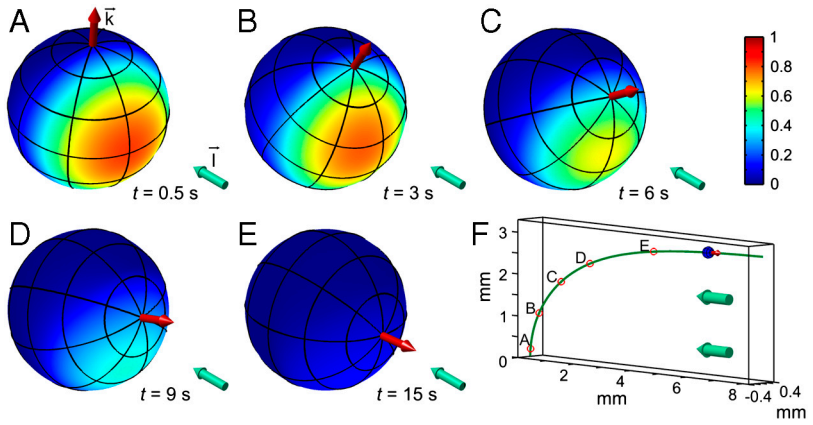

Fig. S8. The behavior of the photoresponse $p(\theta,\phi,t)$ during a phototactic turn, using the full model defined in the main text, neglecting bottom-heaviness. *A–E* show the colony axis (*Red Arrow*) tipping toward the direction of light (*Aqua Arrow*) over time. The color scheme illustrates the magnitude of p. *F* shows the location of colonies in *A–E* along the swimming trajectory.